

The Trispectrum as a Diagnostic of Primordial Orthogonal non-Gaussianities

Sébastien Renaux-Petel

Laboratoire de Physique Théorique et Hautes Energies, Institut Lagrange de Paris, University Paris 6, 4 place Jussieu, Paris, France

E-mail: srenaux@lpthe.jussieu.fr

Abstract. In single-field inflationary models with a low sound speed, the orthogonal shape of the primordial bispectrum arises due to partial cancellations between equilateral-type shapes. This fact allows for a speed of sound c_s as low as about 0.01, which is actually weakly preferred by WMAP data. For such values, the trispectrum, scaling like $1/c_s^4$, is of order 10^8 and is therefore comparable to, and greater than, the 1σ observational bound $t_{NL}^{\text{eq}} = (-3.11 \pm 7.5) \times 10^6$. Hence, the trispectrum is already constraining inflationary mechanisms candidates for generating an orthogonal bispectrum at the level hinted in WMAP data. If this signal persists in imminent Planck data, most of the parameter space of the simplest effective field theory of inflation will be under observational pressure, while a dedicated analysis will be needed for the substantial fraction of parameter space where we show that a qualitatively new, orthogonal, trispectrum naturally arises.

Keywords: inflation, non-gaussianity, cosmological parameters from CMBR

Contents

1	Introduction	1
2	The trispectrum from low sound speed models	3
2.1	The effective field theory of inflation up to quartic order	3
2.2	The trispectrum	5
3	‘Equilateral’ and orthogonal trispectra.	6
3.1	Results	6
3.2	Shapes of trispectra	9
4	Conclusions	11
A	Comparison between orthogonal trispectra	14

1 Introduction

The deviation from perfect Gaussian statistics of the primordial curvature perturbation ζ enables one to discriminate amongst the candidate physical mechanisms that produced the seed primordial fluctuations (see for instance [1–5] for recent reviews). In this respect, it is fair to say that, despite significant efforts, the trispectrum has received considerably less attention than the bispectrum, in particular concerning data analysis. To our knowledge, three types of constraints on well motivated primordial trispectra are now available¹: constraints on τ_{NL} and g_{NL} [6, 7] – which set the amplitude of the two different trispectra generated classically on super-Hubble scales in early-universe models with multiple degrees of freedom – and constraints on t_{NL}^{eq} [6], setting the amplitude of a representative ‘equilateral-type’ trispectrum, generated by quantum interactions around Hubble crossing. The latter parameter is the equivalent for the trispectrum of f_{NL}^{eq} for the bispectrum, while the former are the counterparts of f_{NL}^{loc} . Another important type of primordial bispectrum constrained by data, orthogonal non-Gaussianities [8], has up to now no counterpart at the level of the trispectrum.

The purpose of the present paper is two-fold. Our first aim is to show that an ‘orthogonal-type’ trispectrum naturally arises in a significant fraction of parameter space in the simplest theoretical context (to be more accurate, this is a one-parameter family of

¹Reference [6] constrains as well the non-primordial trispectrum signal induced by cosmic strings, as well as the primordial constant model, which provides a useful benchmark, but which has no physical motivation yet.

trispectra as we will see). Our second, related, aim, is to point out the use of the trispectrum as a useful diagnostic for the appearance of a large bispectrum of the orthogonal type.

In particular, the final WMAP data [9] indicated a 2.45σ hint of orthogonal non-Gaussianities: $-445 < f_{NL}^{\text{orth}} < -45$ (95% *CL*) (while showing no evidence of equilateral non-Gaussianities: $-221 < f_{NL}^{\text{eq}} < 323$ (95% *CL*)). When interpreted in terms of the effective field theory of inflation [8, 10], the orthogonal shape arises from partial cancellations between otherwise equilateral shapes² (see [12, 13] for the first concrete realization of this mechanism), leading to a smaller amplitude than the general estimate $f_{NL} \sim 1/c_s^2$, namely $f_{NL}^{\text{orth}} = \mathcal{O}(\frac{0.01}{c_s^2})$. This fact allows for a speed of sound c_s as low as about 0.01, which is actually (weakly) preferred by current data [9] (see Fig. 1). For such values of c_s , and unless inflation occurred in the region of parameter space where similar partial cancellations that leads to the orthogonal bispectrum arises at the level of the trispectrum, the amplitude of the trispectrum, scaling as $1/c_s^4$, is of order 10^8 and hence is already comparable to (and greater than) current constraints $t_{NL}^{\text{eq}} = (-3.11 \pm 7.5) \times 10^6$ obtained with WMAP data [6]. We will make this more quantitative in the body of this paper, but our message is simple: the trispectrum is already constraining inflationary mechanisms candidates for generating an orthogonal bispectrum at the level hinted in WMAP data. If this signal persists in imminent Planck data, most of the parameter space of the simplest effective field theory of inflation will be under strain, while a dedicated analysis of our orthogonal trispectrum signal will be needed for the remaining one.

The plan of our paper is as follows. In section 2, we use the effective field theory of inflation at the single-derivative level to parametrize the cubic and quartic action for fluctuations in low sound speed models. We then give the expression of the trispectrum generated in these models, using the results of Chen *et al* [14] in the setup of k-inflation [15, 16], which is computationally equivalent. The overall amplitude of this trispectrum is fixed by the speed of sound c_s , while its shape depends on two-parameters: A , which determines the shape of the bispectrum, and B , which is unrelated in general. Section 3 is then dedicated to the study of the resulting 2-parameter family of shapes of trispectra in the region of parameter space $3.1 \lesssim A \lesssim 4.2$ where the orthogonal bispectrum is generated and where values of the speed of sound as low as $\mathcal{O}(0.01)$ are allowed. We define the region of parameter space where the trispectrum can be well represented by the ‘equilateral’ one and is thus already constrained by present data, and represent the new shape that arises in the complementary region. We conclude in section 4.

²Recently, a bispectrum with a significant overlap with the orthogonal shape was shown to arise in a different context [11].

2 The trispectrum from low sound speed models

In this section, we give the expression of the leading-order trispectrum generated in the simplest set-up of the effective field theory of inflation, which is computationally equivalent to k-inflation. Readers who are familiar with both the effective field theory of inflation and the trispectrum generated in low sound speed models can skip this section and proceed directly to section 3.

2.1 The effective field theory of inflation up to quartic order

In this subsection, we briefly review the effective field theory of inflation developed in [10], or to be more accurate the effective field theory of fluctuations generated in single-clock inflation. In such models with only one non-gravitational degree of freedom, it is always possible to choose a slicing such that surfaces of constant t coincide with surfaces where the ‘clock’ is unperturbed, *i.e.* such that $\delta\phi(t, \mathbf{x}) = 0$ in the case of a scalar field clock. No explicit scalar fluctuations appear in this unitary gauge in which time diffeomorphisms have been fixed. The most generic effective action in this gauge can thus be built by allowing only metric operators invariant under the unbroken time-dependent spatial reparametrizations. It can then be shown that considering fluctuations around a spatially flat FLRW background amounts to studying the following action [10]

$$S = \int d^4x \sqrt{-g} \left[\frac{M_{\text{Pl}}^2}{2} R + M_{\text{Pl}}^2 \dot{H} g^{00} - M_{\text{Pl}}^2 (3H^2 + \dot{H}) + F(\delta g^{00}, \delta K_{\mu\nu}, \delta R_{\mu\nu\rho\sigma}; \nabla_\mu; t) \right]$$

where H is the Hubble parameter, $\delta g^{00} \equiv g^{00} + 1$, $\delta K_{\mu\nu}$ (respectively $\delta R_{\mu\nu\rho\sigma}$) is the fluctuation of the extrinsic curvature of constant time surfaces (respectively of the 4-dimensional Riemann tensor) and where F starts quadratic in its arguments δg^{00} , $\delta K_{\mu\nu}$ and $\delta R_{\mu\nu\rho\sigma}$. The simplest effective field theory at lowest order in derivatives corresponds then to allowing operators involving powers of δg^{00} only, namely, up to quartic order in fluctuations,

$$F = \frac{1}{2} M_2(t)^4 (\delta g^{00})^2 + \frac{1}{3!} M_3(t)^4 (\delta g^{00})^3 + \frac{1}{4!} M_4(t)^4 (\delta g^{00})^4. \quad (2.1)$$

The true effectiveness of this approach relies on the gravitational analogue of the equivalence theorem for the longitudinal components of a massive gauge boson [17]: the scalar degree of freedom can be explicitly reintroduced in the Stückelberg trick, thus restoring full time-diffeomorphism invariance, and it decouples from the gravitational sector at high enough energies, allowing to neglect the complications of the mixing with gravity. In this decoupling regime, the effect of the Stückelberg time diffeomorphism $t \rightarrow t + \pi(x)$ on δg^{00} is simply

$$\delta g^{00} \rightarrow -2\dot{\pi} - \dot{\pi}^2 + \frac{(\partial_i \pi)^2}{a^2}, \quad (2.2)$$

while one can neglect the terms introduced by the time dependence of the $M_n(t)$ at leading order in a slow-varying approximation, or equivalently by assuming that π enjoys an approximate shift-symmetry. The resulting Lagrangian reads, up to quartic order in π :

$$S_{\text{DL}} = \int d^4x \sqrt{-g} \left[M_{\text{Pl}}^2 \dot{H} (\partial_\mu \pi)^2 + 2M_2^4 \left(\dot{\pi}^2 - \dot{\pi} (\partial_\mu \pi)^2 + \frac{1}{4} ((\partial_\mu \pi)^2)^2 \right) + \frac{2M_3^4}{3} (-2\dot{\pi}^3 + 3\dot{\pi}^2 (\partial_\mu \pi)^2) + \frac{2M_4^4}{3} \dot{\pi}^4 \right] \quad (2.3)$$

where $(\partial_\mu \pi)^2 \equiv -\dot{\pi}^2 + (\partial_i \pi)^2/a^2$ is evaluated on the background metric and π is related to the curvature perturbation by the simple relation $\zeta = -H\pi$ at linear order and at leading order in a slow-varying approximation. A non-zero M_2 introduces both a reduced sound speed c_s , such that

$$\frac{1}{c_s^2} - 1 \equiv -\frac{2M_2^4}{M_P^2 \dot{H}}, \quad (2.4)$$

and large cubic and quartic interactions. By introducing $A/c_s^2 \equiv -1 + \frac{2}{3} \left(\frac{M_3}{M_2} \right)^4$, following the WMAP notation in [9], and

$$\frac{B}{2c_s^4} \equiv 1 - \left(\frac{M_3}{M_2} \right)^4 + \frac{1}{2} \left(\frac{M_3}{M_2} \right)^8 - \frac{1}{6} \left(\frac{M_4}{M_2} \right)^4, \quad (2.5)$$

the decoupling Lagrangian can be cast in the form

$$S_{\text{DL}} = \int d^4x \sqrt{-g} \left[-\frac{M_P^2 \dot{H}}{c_s^2} \left(\dot{\pi}^2 - c_s^2 \frac{(\partial_i \pi)^2}{a^2} \right) + \frac{M_P^2 \dot{H}}{c_s^2} \left(\frac{\dot{\pi} (\partial_i \pi)^2}{a^2} + \frac{A}{c_s^2} \dot{\pi}^3 \right) - \frac{M_P^2 \dot{H}}{c_s^2} \left(\frac{((\partial_i \pi)^2)^2}{4a^4} + \frac{3A}{2c_s^2} \dot{\pi}^2 \frac{(\partial_i \pi)^2}{a^2} + \frac{(9A^2/4 - B)}{c_s^4} \dot{\pi}^4 \right) \right] \quad (2.6)$$

where we have kept leading-order terms in the interesting limit $c_s^2 \ll 1$ of a large bispectrum. As explained in [8], A of order one is technically natural from the effective field point of view as the operators in $\dot{\pi}^3$ and $\dot{\pi} (\partial_i \pi)^2$ then introduce the same strong coupling scale. The same reasoning shows that B of order one is technically natural as well. Note also that, as the effective field theory of inflation with operators involving only powers of δg^{00} is computationally equivalent to k-inflation, it should not come as a surprise that the Lagrangian (2.6) can be identified with the one in [14, 18] (see also [19]), with the correspondence, at leading order in $1/c_s^2$:

$$\frac{A}{c_s^2} \leftrightarrow -2 \frac{\lambda}{\Sigma}, \quad \frac{B}{c_s^4} \leftrightarrow \frac{\mu}{\Sigma} - 9 \frac{\lambda^2}{\Sigma^2}. \quad (2.7)$$

Note eventually that DBI inflation [20, 21] simply corresponds to $A = -B = -1$ in our parametrization.

2.2 The trispectrum

Using the correspondence (2.7), the primordial trispectrum generated from the inflationary fluctuations Lagrangian (2.6) can be simply read off from the equivalent result Eq. (3.32) in [14], namely

$$\langle \zeta(\mathbf{k}_1)\zeta(\mathbf{k}_2)\zeta(\mathbf{k}_3)\zeta(\mathbf{k}_4) \rangle_c = (2\pi)^9 \mathcal{P}_\zeta^3 \delta\left(\sum_i \mathbf{k}_i\right) \prod_{i=1}^4 \frac{1}{k_i^3} \mathcal{T}(k_1, k_2, k_3, k_4, k_{12}, k_{14}) \quad (2.8)$$

where $k_{ij} = |\mathbf{k}_i + \mathbf{k}_j|$,

$$\mathcal{T}(A, B) = \frac{1}{c_s^4} \left(\frac{A^2}{4} T_{s1} - \frac{A}{2} T_{s2} + T_{s3} - B T_{c1} \right), \quad (2.9)$$

$$T_{c1} = 36 \frac{(k_1 k_2 k_3 k_4)^2}{(k_1 + k_2 + k_3 + k_4)^5} \quad (2.10)$$

and where the explicit (lengthy) expressions of T_{s1}, T_{s2}, T_{s3} can be found in [14]. Note that although the operators in $((\partial_i \pi)^2)^2$ and $\dot{\pi}^2 (\partial_i \pi)^2$ in Eq. (2.6) are of the same order as the one in $\dot{\pi}^4$, they cancel in the quartic Hamiltonian at leading order in the small sound speed limit, leaving only the scalar exchange contributions T_{si} and the contact-interaction trispectrum T_{c1} generated from the operator in $\dot{\pi}^4$.

A detailed analysis of the shapes of the four constituent trispectra in (2.9) was performed in [14], to which we refer the reader for more details (see also [19]). Overall, they reached the conclusion that they all share very similar properties. In particular, as expected from trispectra of quantum origin generated around the time of Hubble crossing, they are the largest for the configurations where both the external and internal momenta are of similar magnitude, *i.e.* near the regular tetrahedron (RT) limit where $k_1 = k_2 = k_3 = k_4 = k_{12} = k_{14}$. This similarity was used in [6] in which observational constraints on the simple and representative ‘equilateral-type’ trispectrum T_{c1} were derived (the only observational constraint on a trispectrum from quantum origin to date). However, we are interested here in the possible cancellations between these overall similar shapes, as we vary the parameters (A, B) , which could result in a trispectrum poorly correlated with T_{c1} , and to which current constraints would hence be blind. As we have explained in the introduction, of particular interest is the region (weakly) favored by WMAP nine-year data $3.1 \lesssim A \lesssim 4.2$ where partial cancellations between the operators $\dot{\pi}(\partial_i \pi)^2$ and $\dot{\pi}^3$ in (2.6) leads to a primordial bispectrum correlated with the orthogonal template at more than 80 % [8], and in which a low sound speed of order 0.01 is allowed [9] (see Fig. 1). We present the results of such a study in the following section.

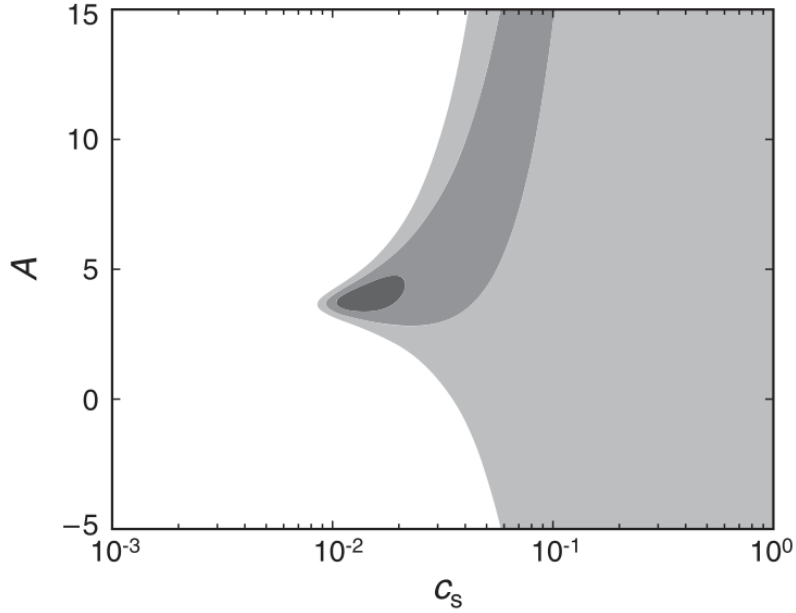


Figure 1. WMAP nine-year constraints: 1σ , 2σ and 3σ confidence regions derived from the bispectrum on the sound speed c_s and interaction coefficient A in Eq. (2.6). Figure taken from [9].

3 ‘Equilateral’ and orthogonal trispectra.

3.1 Results

As we have just explained in the preceding section, we would like to assess where in parameter space the overall trispectrum (2.9) can/cannot be well represented by the simple ‘equilateral-type’ trispectrum T_{c1} constrained by data. Given the expression (2.9), it is clear that, for any A , the trispectrum interpolates between highly correlated and highly anti-correlated with T_{c1} as we vary B from large negative to large positive values. A qualitatively new shape should hence arise in the neighborhood of a particular value of B . The only questions are then: around which value? How narrow is this region? What the new shape looks like? And how much does the latter vary with A ? in particular in the region $3.1 \lesssim A \lesssim 4.2$.

To answer these questions, one should ultimately resort to the scalar product defined by the estimator used to constrain the primordial trispectra, for instance the correlator [22, 23]

$$F[T, T'] = \sum_{l_i, L} \frac{T_{l_3 l_4}^{l_1 l_2}(L) T_{l_3 l_4}'^{l_1 l_2}(L)}{(2L+1) C_{l_1} C_{l_2} C_{l_3} C_{l_4}} \quad (3.1)$$

between angular trispectra when using the CMB as the observational probe. Implementing such a correlator is however beyond the scope of this paper. We rather stuck to representing 2-dimensional slices of our trispectra in different representative limits, as was originally done in [14]. Note that we actually did make use of quantitative correlators, in Fourier-space, using reduced trispectra [23, 24] or full trispectra [25]. However, we found these correlators to be somewhat misleading for our purpose, as they indicated widely different regions of parameter space as giving rise to an ‘orthogonal’ trispectrum, in the sense of a trispectrum with a small correlation with T_{c1} . Moreover, when visually representing these candidate orthogonal trispectra, they appeared almost indistinguishable from T_{c1} . On the contrary, we believe that our procedure is trustworthy and sufficient to define where T_{c1} represents well or not the overall trispectrum (2.9), and, as we will explain below, we have quantitative arguments that support our findings.

To summarize the latter, we find that, for the three representative values $A = \{3.2, 3.6, 4\}$ in the interesting range $3.1 \lesssim A \lesssim 4.2$, the total trispectrum (2.9) can be well represented by T_{c1} only for

- $B \lesssim 5$ and $B \gtrsim 11$ ($A = 3.2$) (3.2)

- $B \lesssim 5$ and $B \gtrsim 14$ ($A = 3.6$) (3.3)

- $B \lesssim 10$ and $B \gtrsim 19$ ($A = 4$) (3.4)

while a qualitatively different shape arises in the complementary region, centered around the values

- $B \simeq 8.5$ ($A = 3.2$) (3.5)

- $B \simeq 11.5$ ($A = 3.6$) (3.6)

- $B \simeq 14.5$ ($A = 4$) (3.7)

Moreover, we find that the shapes of these various orthogonal trispectra depend very weakly on A and can thus be well represented by (up to an overall multiplicative factor)

$$\mathcal{T}_{\text{orth}} = 3.2 T_{s1} - 1.8 T_{s2} + T_{s3} - 11.5 T_{c1} , \quad (3.8)$$

corresponding to the values $A = 3.6, B = 11.5$.

Quantitatively, a simple measure of the amplitude of the trispectrum is given by the parameter t_{NL} defined such that

$$\frac{1}{k^3} \mathcal{T}(k_1, k_2, k_3, k_4, k_{12}, k_{14}) \xrightarrow[\text{limit}]{\text{RT}} t_{NL} , \quad (3.9)$$

where RT stands for the regular tetrahedron limit $k_1 = k_2 = k_3 = k_4 = k_{12} = k_{14} \equiv k$. Applied to (2.9), this gives

$$t_{NL} = \frac{1}{c_s^4} (0.062A^2 - 0.210A + 0.305 - 0.035B) . \quad (3.10)$$

The observational constraint relevant for our purpose in [6] is derived by assuming that \mathcal{T} in Eq. (2.8) can be well approximated by T_{c1} in (2.10), *i.e.* it puts a bound on the parameter t_{NL}^{eq} defined such that $\mathcal{T} = t_{NL}^{\text{eq}}/t_{NL}(T_{c1}) \times T_{c1}$. It is therefore applicable only in the ranges defined in Eqs. (3.2)-(3.4) where the trispectrum becomes essentially proportional to T_{c1} . To make the link with the observational constraints on the bispectrum, let us apply this to the value of the speed of sound $c_s = 0.013^3$ such that $f_{NL}^{\text{orth}} = -245$ (the central WMAP estimate) for the representative value $A = 3.6$. One then finds

$$t_{NL} = 1.17 \times 10^7 \times (1 - 0.098B) \quad (3.11)$$

which is comparable to (and actually greater than) the 1σ constraint [6]

$$t_{NL}^{\text{eq}} = (-3.11 \pm 7.5) \times 10^6 . \quad (3.12)$$

Similar numbers are of course found in the range $3.1 \lesssim A \lesssim 4.2$: $t_{NL} = 1.62 \times 10^7 \times (1 - 0.098B)$ for $A = 3.2$ and $t_{NL} = 8.80 \times 10^6 \times (1 - 0.098B)$ for $A = 4$, under the same hypotheses. There is currently no point in performing a more detailed statistical analysis given the weak 2.45σ hint of an orthogonal bispectrum, but we believe our message is clear: the trispectrum is already constraining candidate low sound speed inflationary models generating an orthogonal bispectrum at the level suggested in WMAP data. For instance, the result Eq. (3.11) is 2.13σ (respectively 3.50σ) away from the central value Eq. (3.12) for $B = -1$ (respectively $B = -10$). Even a decrease in the error bar by a factor of a few, as expected from Planck [26], could hence constrain these scenarios in a statistically significant way, provided of course that the orthogonal bispectrum signal is confirmed.

Note once again that Eq. (3.11) can be meaningfully compared to the observational constraint (3.12) only for $B \lesssim 5$ and $B \gtrsim 14$. In the intermediate range, a shape qualitatively different from T_{c1} arises to which current constraints are mostly blind. Relatedly, the fact that t_{NL} in Eq. (3.11) vanishes for $B = 10.20$, so in the middle of this intermediate range, and close to the value $B = 11.5$ at which we defined our representative orthogonal trispectrum, justifies *a posteriori* our procedure and our findings. Indeed, t_{NL} measures the amplitude of equilateral-type shapes, which peak around the regular tetrahedron limit. The fact that it vanishes does not indicate that no significant non-Gaussianities are generated, but rather that they can not be faithfully represented by the ‘equilateral’ ansatz

³This value of c_s is found using Eq. 57 in Ref. [9].

T_{c1} in Eq. (2.10) The estimator t_{NL} in Eq. (3.10) vanishes as well at $B = 7.76$ for $A = 3.2$ and at $B = 13.21$ for $A = 4$, so again in the intermediate ranges that we defined and close to the values $B \simeq 8.5$ and $B \simeq 14.5$ at which defined the appearance of the orthogonal trispectrum.

Eventually, let us stress that the origin of our representative orthogonal trispectrum Eq. (3.8) is not an ad-hoc orthogonalization procedure: by subtracting out the similarities between T_{c1} , T_{s1} , T_{s2} and T_{s3} , one can indeed imagine the construction of a basis of the vector space spanned by these four trispectra constituted by T_{c1} and three qualitatively different and mutually orthogonal trispectra. While mathematically correct, this procedure would be somewhat artificial. On the contrary, we have shown the natural appearance of trispectra qualitatively different from the equilateral one T_{c1} , and which can be represented by the template Eq. (3.8), in a substantial fraction of parameter space in the simplest theoretical context.

3.2 Shapes of trispectra

In this subsection, we show plots of T_{c1} and of $\mathcal{T}(3.6, B)$ supporting the results stated above, namely that the latter can be represented to a good approximation by T_{c1} for $B \lesssim 5$ and $B \gtrsim 14$, and that a trispectrum qualitatively different from T_{c1} arises near $B = 11.5$. We leave other plots, in particular for other values of A , to the appendix A.

Our scale invariant trispectra are in general functions of 5 variables, and in what follows, we follow Ref. [14] and represent 2-dimensional slices of them in different representative limits. A slight difference is that we chose to plot the scale-independent quantities $\tilde{\mathcal{T}} = \mathcal{T}/(k_1 k_2 k_3 k_4)^{3/4}$ rather than \mathcal{T} itself (we have checked that similar conclusions are reached by using the two sets). The four limits we consider are:

- The specialized planar limit, in which $k_1 = k_3 = k_{14}$, and the tetrahedron reduces to a planar quadrangle with [14]

$$k_{12} = \left[k_1^2 + \frac{k_2 k_4}{2k_1^2} \left(k_2 k_4 + \sqrt{(4k_1^2 - k_2^2)(4k_1^2 - k_4^2)} \right) \right]^{1/2}. \quad (3.13)$$

Shapes are then represented as functions of k_2/k_1 and k_4/k_1 .

- Near the double-squeezed limit: $k_3 = k_4 = k_{12}$ and the tetrahedron is a planar quadrangle with [14]

$$k_2 = \frac{\sqrt{k_1^2 (-k_{12}^2 + k_3^2 + k_4^2) - k_{s1}^2 k_{s2}^2 + k_{12}^2 k_{14}^2 + k_{12}^2 k_4^2 + k_{14}^2 k_4^2 - k_{14}^2 k_3^2 - k_4^4 + k_3^2 k_4^2}}{\sqrt{2} k_4}, \quad (3.14)$$

where k_{s1} and k_{s2} are defined as

$$\begin{aligned} k_{s1}^2 &\equiv 2\sqrt{(k_1 k_4 + \mathbf{k}_1 \cdot \mathbf{k}_4)(k_1 k_4 - \mathbf{k}_1 \cdot \mathbf{k}_4)} , \\ k_{s2}^2 &\equiv 2\sqrt{(k_3 k_4 + \mathbf{k}_3 \cdot \mathbf{k}_4)(k_3 k_4 - \mathbf{k}_3 \cdot \mathbf{k}_4)} . \end{aligned} \quad (3.15)$$

Shapes are then represented as functions of k_4/k_1 and k_{14}/k_1 .

- The folded limit: $k_{12} = 0$, hence $k_1 = k_2$ and $k_3 = k_4$. Shapes are then represented as functions of k_4/k_1 and k_{14}/k_1 , and we assumed $k_4 < k_1$ without loss of generality.
- The equilateral limit: $k_1 = k_2 = k_3 = k_4$. Shapes are then represented as functions of k_{12}/k_1 and k_{14}/k_1 .

In Figs. 2, 3 and 4, we represent the shape functions of \tilde{T}_{c1} (top left), $\tilde{\mathcal{T}}(3.6, 11.5)$ (top right), $\tilde{\mathcal{T}}(3.6, 5)$ (bottom left) and $-\tilde{\mathcal{T}}(3.6, 14)$ (bottom right), in the specialized planar limit, near the double-squeezed limit and in the folded limit respectively. The shape functions are left white when the momenta do not form a tetrahedron. From these plots, it is evident that $\tilde{\mathcal{T}}(3.6, 5)$ (respectively $\tilde{\mathcal{T}}(3.6, 14)$) is well correlated (respectively anti-correlated) with \tilde{T}_{c1} , while $\tilde{\mathcal{T}}(3.6, 11.5)$ is qualitatively different from it. Note that the scales are different in each plot, and that $\tilde{\mathcal{T}}(3.6, 11.5)$ has both positive and negative values. In these three limits, the tetrahedron reduces to a planar quadrangle, which is the configuration probed by the CMB (see [23]). In Fig. 5, the non-planar, equilateral, limit, is also displayed. \tilde{T}_{c1} is constant in this limit, so that its effect in Eq. (2.9) is simply an overall shift in amplitude. For this reason, we represent only \tilde{T}_{c1} (left) and $\tilde{\mathcal{T}}(3.6, 11.5)$ (right).

Eventually, note that for $A \lesssim 3.1$ and $A \gtrsim 4.2$, the bispectrum is of equilateral type and observationally allowed values of the speed of sound c_s are greater than in the range $3.1 \lesssim A \lesssim 4.2$, of order $c_s \gtrsim 0.1$ [9] (see Fig. 1). The trispectrum (2.9) is then of maximum amplitude $\mathcal{O}(10^4)$ and, for such values, is not expected to be efficiently constrained by CMB data [27]. It is nonetheless interesting to investigate the appearance of orthogonal-type trispectra in this region of parameter space. We have not performed an exhaustive study of this, but the reasonings made in subsection 3.1 show that a trispectrum qualitatively different from T_{c1} arises around a certain value of B for any A , and that the cancellation of the estimator t_{NL} in Eq. (3.10) is a good estimate of where this arises, leading to the one-parameter family of approximate orthogonal trispectra

$$\frac{A^2}{4} T_{s1} - \frac{A}{2} T_{s2} + T_{s3} - 8.66 (1 - 0.69A + 0.20A^2) T_{c1} . \quad (3.16)$$

We have visually checked that this indeed the case, and moreover that outside the range $3.1 \lesssim A \lesssim 4.2$, these trispectra can differ substantially from our representative orthogonal trispectrum Eq. (3.8).

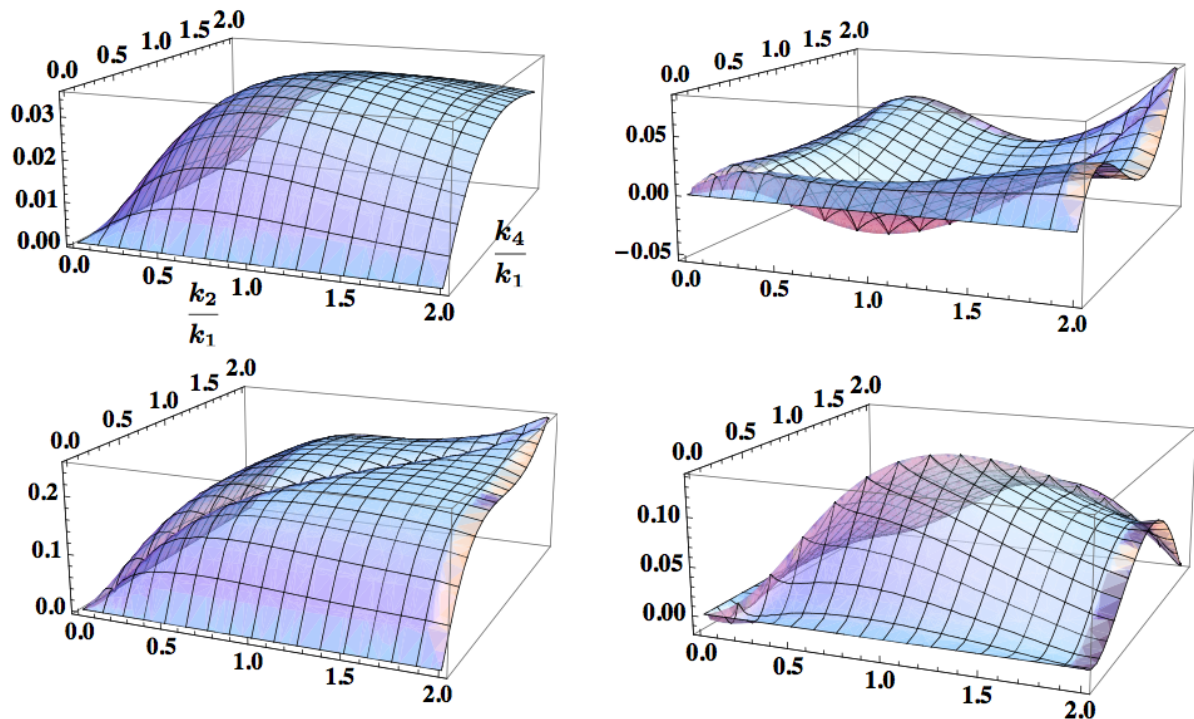


Figure 2. In this group of figures, we consider the specialized planar limit with $k_1 = k_3 = k_{14}$, and plot \tilde{T}_{c1} (top left), $\tilde{T}(3.6, 11.5)$ (top right), $\tilde{T}(3.6, 5)$ (bottom left) and $-\tilde{T}(3.6, 14)$ (bottom right) as functions of k_2/k_1 and k_4/k_1 .

4 Conclusions

Amongst the three template bispectra constrained by the WMAP team, the orthogonal shape has been much less studied than local or equilateral non-Gaussianities. Although not statistically significant, the 2.45σ hint of orthogonal bispectrum indicated by the final data [9] hence deserves close attention. Observational consistency checks have been performed in [9], showing no obvious source of systematic contamination. The purpose of this paper was to show that the trispectrum is already providing another important consistency check, and that it actually puts under strain some of the simplest inflationary mechanisms generating such a signal. The reason is simple: when interpreted in the theoretical framework of the effective field theory of single-clock inflation, the WMAP signal favors a value of the sound speed of inflaton fluctuations of order $\mathcal{O}(0.01)$. For such low values, the trispectrum, scaling like $1/c_s^4$, is generically of order 10^8 , and hence is comparable to, and greater than, the current 1σ observational bound $t_{NL}^{\text{eq}} = (-3.11 \pm 7.5) \times 10^6$ [6].

This limit is derived under the assumption that the trispectrum generated in low

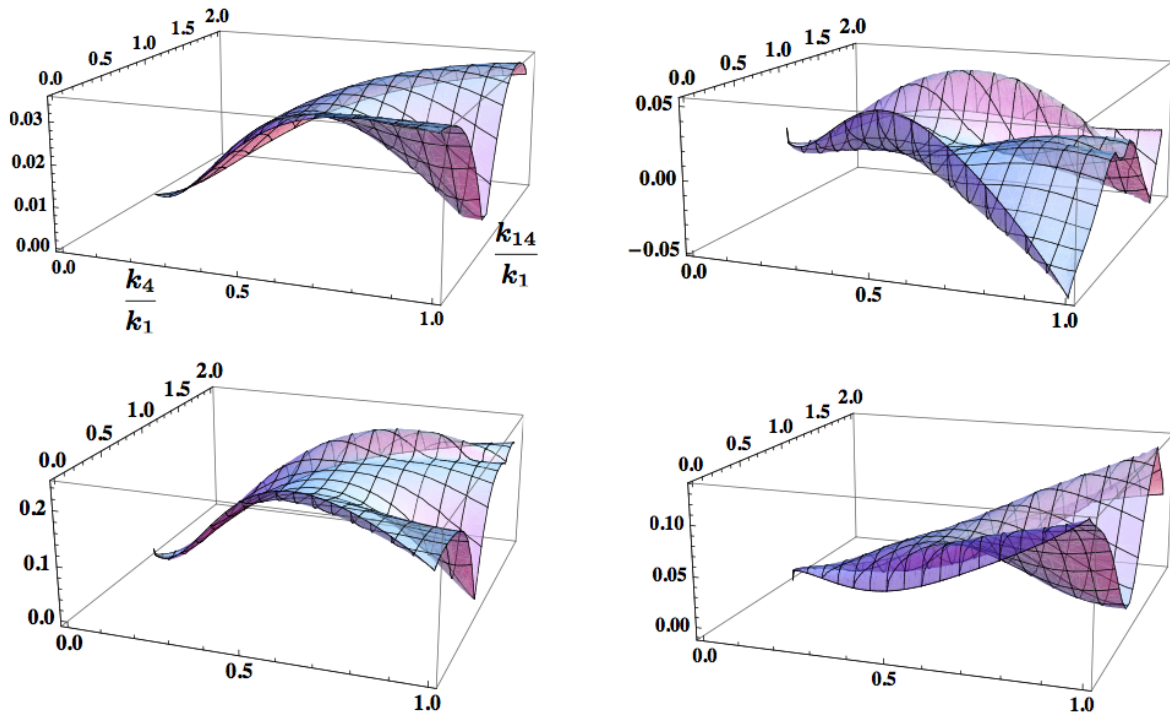


Figure 3. In this group of figures, we look at the shapes near the double squeezed limit: we consider the case where $k_3 = k_4 = k_{12}$ and the tetrahedron is a planar quadrangle. We plot \tilde{T}_{c1} (top left), $\tilde{T}(3.6, 11.5)$ (top right), $\tilde{T}(3.6, 5)$ (bottom left) and $-\tilde{T}(3.6, 14)$ (bottom right) as functions of k_4/k_1 and k_{14}/k_1 .

sound speed models can be well approximated by the simple ‘equilateral-type’ shape generated by the operator $\hat{\pi}^4$. While this is true in a large fraction of parameter space, we have shown that there exists a non-negligible fraction of it in which qualitatively new shapes naturally arise, to which current constraints are almost blind. In the interesting region in which an orthogonal bispectrum is generated, an essentially unique orthogonal trispectrum Eq. (3.8) can be generated, and it would be interesting to undertake an analysis of CMB data in search for such a signal.

Acknowledgments

We would like to thank Xingang Chen, Paolo Creminelli, Keisuke Izumi, Kazuya Koyama, Shuntaro Mizuno, Guido W. Pettinari, Donough Regan, Filippo Vernizzi and Yi Wang for useful conversations related to the topic of this paper, and especially Keisuke Izumi, Shuntaro Mizuno and Donough Regan for useful explanations about their primordial trispectrum correlators, and Guido W. Pettinari for useful comments on a draft version of

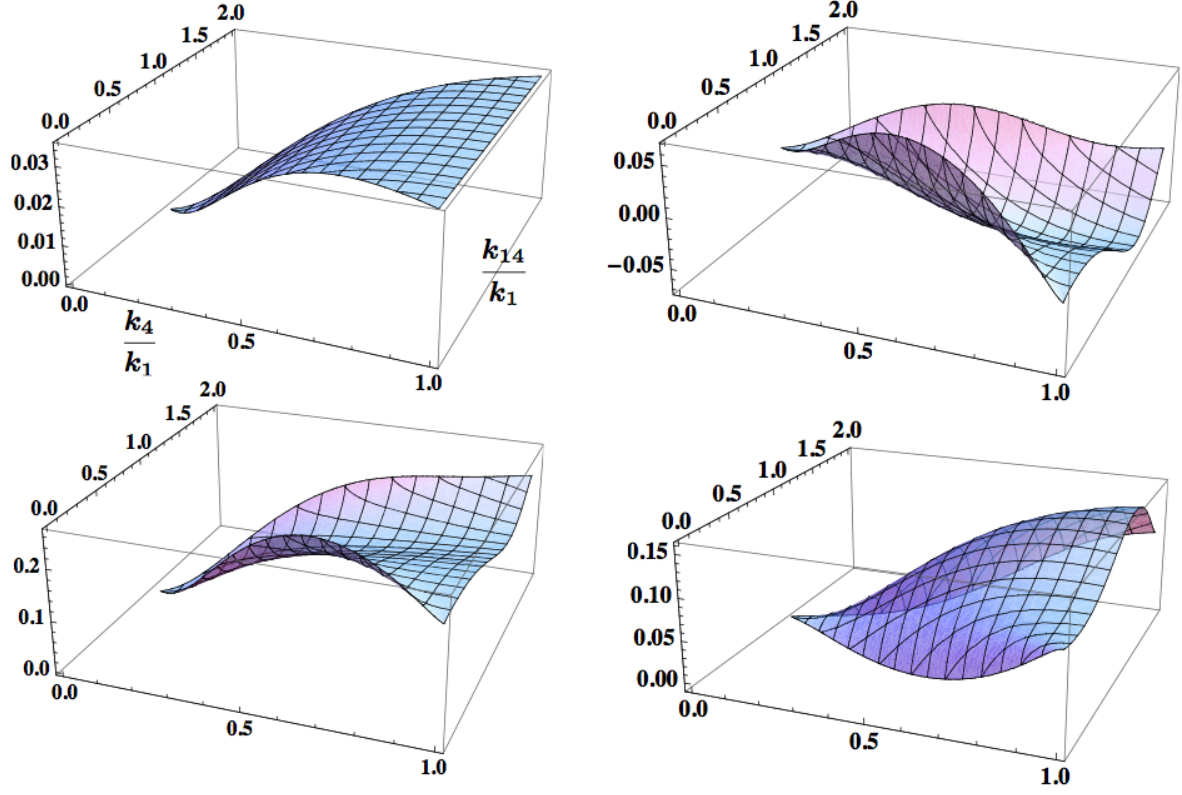


Figure 4. In this group of figures, we consider the folded limit $k_{12} = 0$, and plot \tilde{T}_{c1} (top left), $\tilde{T}(3.6, 11.5)$ (top right), $\tilde{T}(3.6, 5)$ (bottom left) and $-\tilde{T}(3.6, 14)$ (bottom right) as functions of k_4/k_1 and k_{14}/k_1 .

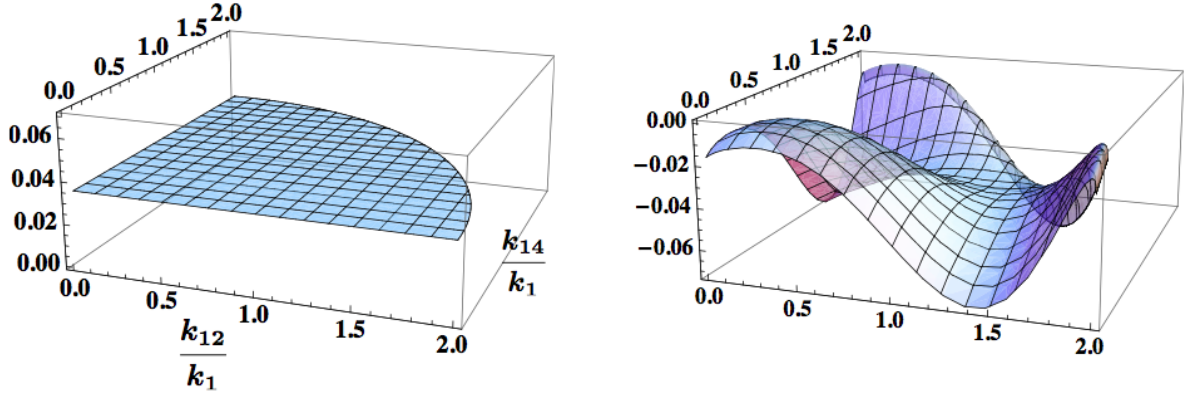


Figure 5. In this group of figures, we consider the equilateral limit $k_1 = k_2 = k_3 = k_4$, and plot \tilde{T}_{c1} (left) and $\tilde{T}(3.6, 11.5)$ (right) as functions of k_{12}/k_1 and k_{14}/k_1 .

this paper. This work was supported by French state funds managed by the ANR within the Investissements d’Avenir programme under reference ANR-11-IDEX-0004-02.

A Comparison between orthogonal trispectra

We have explained in subsection 3.1 that the trispectrum Eq. (3.8) represents well the orthogonal trispectra Eqs. (3.5)-(3.7) arising in the range $3.1 \lesssim A \lesssim 4.2$. In this appendix, we demonstrate this by showing, in Figs. 6, 7, 8 and 9, plots of $\tilde{\mathcal{T}}(3.2, 8.5)$, $\tilde{\mathcal{T}}(3.6, 11.5)$ and $\tilde{\mathcal{T}}(4, 14.5)$ in the same limits as for Figs. 2 to 5. For comparison, we also represent \tilde{T}_{s1} , an ‘equilateral-type’ shape different from \tilde{T}_{c1} , which we have represented in the other figures. The similarity between $\tilde{\mathcal{T}}(3.2, 8.5)$, $\tilde{\mathcal{T}}(3.6, 11.5)$ and $\tilde{\mathcal{T}}(4, 14.5)$ is striking.

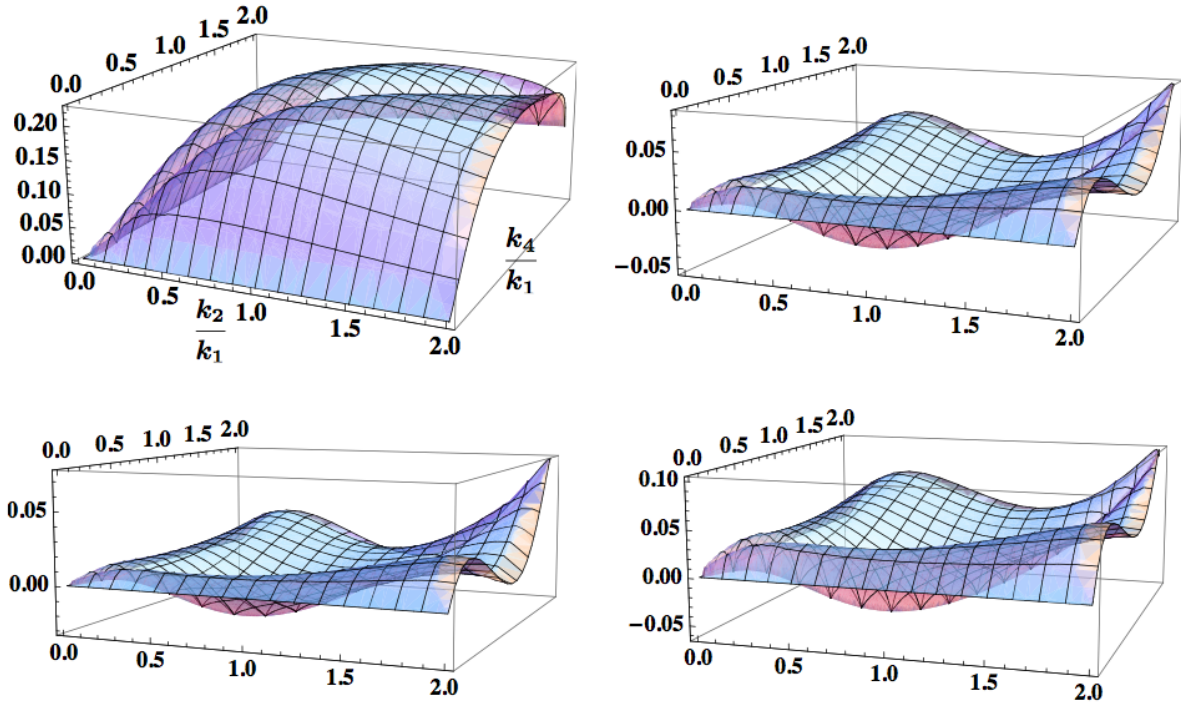


Figure 6. In this group of figures, we consider the specialized planar limit with $k_1 = k_3 = k_{14}$, and plot \tilde{T}_{s1} (top left), $\tilde{\mathcal{T}}(3.6, 11.5)$ (top right), $\tilde{\mathcal{T}}(3.2, 8.5)$ (bottom left) and $\tilde{\mathcal{T}}(4, 14.5)$ (bottom right) as functions of k_2/k_1 and k_4/k_1 .

References

- [1] X. Chen, Adv. Astron. **2010** (2010) 638979 [arXiv:1002.1416 [astro-ph.CO]].

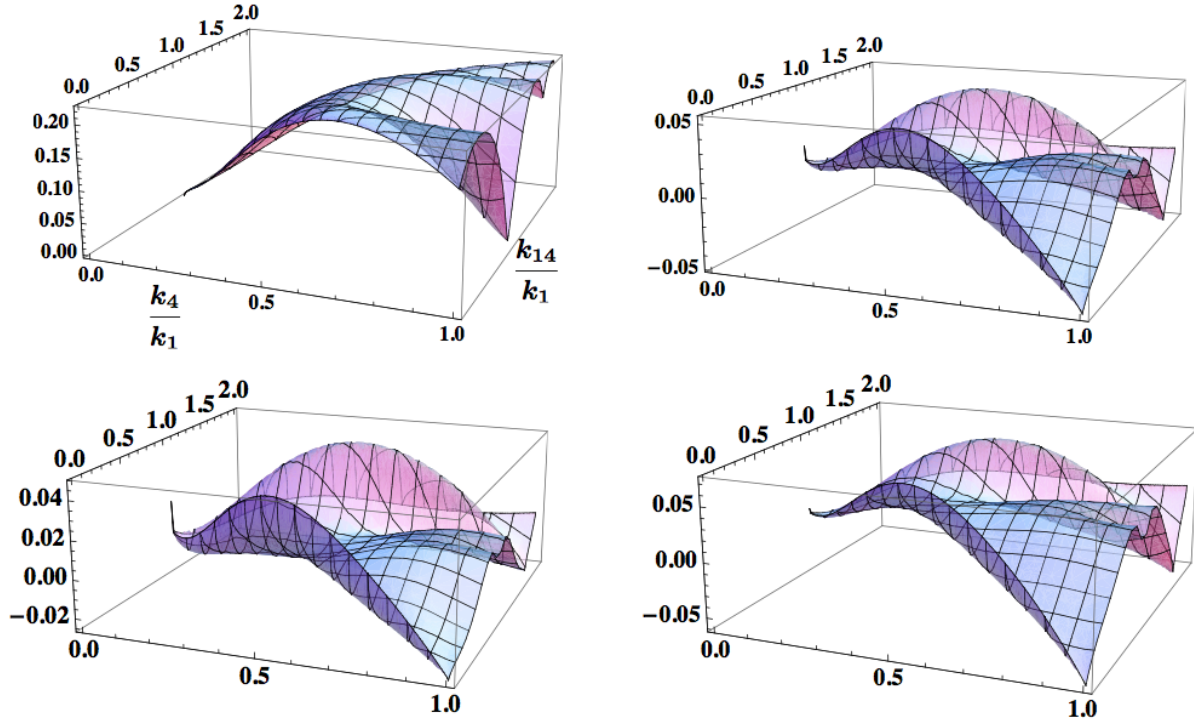


Figure 7. In this group of figures, we look at the shapes near the double squeezed limit: we consider the case where $k_3 = k_4 = k_{12}$ and the tetrahedron is a planar quadrangle. We plot \tilde{T}_{s1} (top left), $\tilde{T}(3.6, 11.5)$ (top right), $\tilde{T}(3.2, 8.5)$ (bottom left) and $\tilde{T}(4, 14.5)$ (bottom right) as functions of k_4/k_1 and k_{14}/k_1 .

- [2] C. T. Byrnes and K. -Y. Choi, Adv. Astron. **2010** (2010) 724525 [arXiv:1002.3110 [astro-ph.CO]].
- [3] D. Wands, Class. Quant. Grav. **27** (2010) 124002 [arXiv:1004.0818 [astro-ph.CO]].
- [4] N. Barnaby, Adv. Astron. **2010** (2010) 156180 [arXiv:1010.5507 [astro-ph.CO]].
- [5] D. Langlois, Prog. Theor. Phys. Suppl. **190** (2011) 90 [arXiv:1102.5052 [astro-ph.CO]].
- [6] J. R. Fergusson, D. M. Regan and E. P. S. Shellard, arXiv:1012.6039 [astro-ph.CO].
- [7] J. Smidt, A. Amblard, C. T. Byrnes, A. Cooray, A. Heavens and D. Munshi, Phys. Rev. D **81** (2010) 123007 [arXiv:1004.1409 [astro-ph.CO]].
- [8] L. Senatore, K. M. Smith and M. Zaldarriaga, JCAP **1001** (2010) 028 [arXiv:0905.3746 [astro-ph.CO]].
- [9] C. L. Bennett, D. Larson, J. L. Weiland, N. Jarosik, G. Hinshaw, N. Odegard, K. M. Smith and R. S. Hill *et al.*, arXiv:1212.5225 [astro-ph.CO].
- [10] C. Cheung, P. Creminelli, A. L. Fitzpatrick, J. Kaplan and L. Senatore, JHEP **0803**

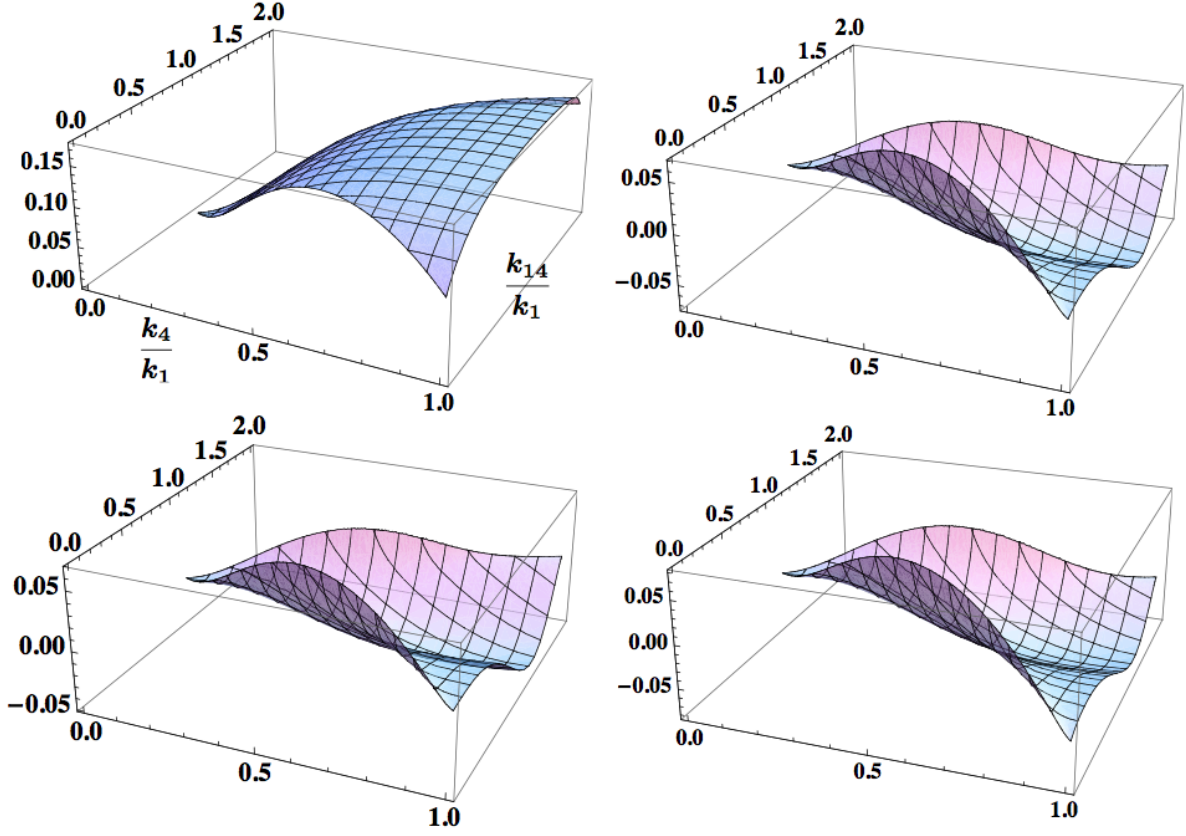


Figure 8. In this group of figures, we consider the folded limit $k_{12} = 0$, and plot \tilde{T}_{s1} (top left), $\tilde{T}(3.6, 11.5)$ (top right), $\tilde{T}(3.2, 8.5)$ (bottom left) and $\tilde{T}(4, 14.5)$ (bottom right) as functions of k_4/k_1 and k_{14}/k_1 .

(2008) 014 [arXiv:0709.0293 [hep-th]].

- [11] D. Green, M. Lewandowski, L. Senatore, E. Silverstein and M. Zaldarriaga, arXiv:1301.2630 [hep-th].
- [12] S. Renaux-Petel, Class. Quant. Grav. **28** (2011) 182001 [Erratum-ibid. **28** (2011) 249601] [arXiv:1105.6366 [astro-ph.CO]].
- [13] S. Renaux-Petel, S. Mizuno and K. Koyama, JCAP **1111** (2011) 042 [arXiv:1108.0305 [astro-ph.CO]].
- [14] X. Chen, B. Hu, M. -x. Huang, G. Shiu and Y. Wang, JCAP **0908** (2009) 008 [arXiv:0905.3494 [astro-ph.CO]].
- [15] C. Armendariz-Picon, T. Damour and V. F. Mukhanov, Phys. Lett. B **458** (1999) 209 [hep-th/9904075].
- [16] J. Garriga and V. F. Mukhanov, Phys. Lett. B **458** (1999) 219 [hep-th/9904176].

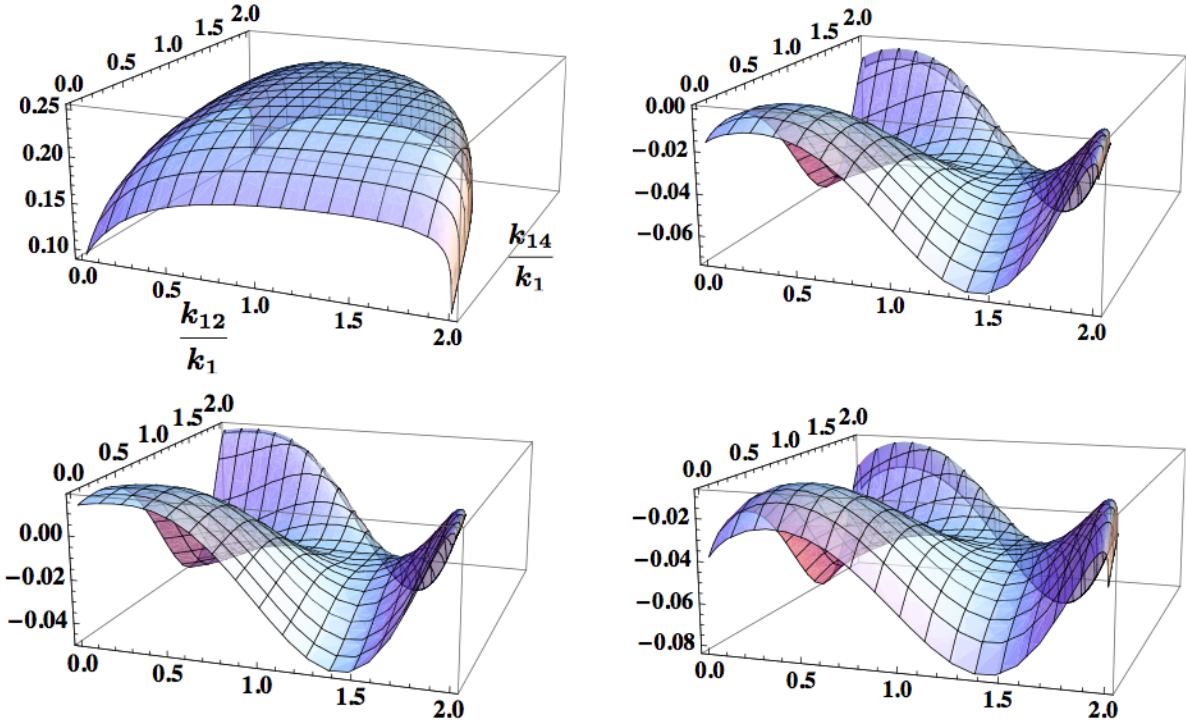


Figure 9. In this group of figures, we consider the equilateral limit $k_1 = k_2 = k_3 = k_4$, and plot \tilde{T}_{s1} (top left), $\tilde{T}(3.6, 11.5)$ (top right), $\tilde{T}(3.2, 8.5)$ (bottom left) and $\tilde{T}(4, 14.5)$ (bottom right) as functions of k_{12}/k_1 and k_{14}/k_1 .

- [17] J. M. Cornwall, D. N. Levin and G. Tiktopoulos, Phys. Rev. D **10** (1974) 1145
[Erratum-ibid. D **11** (1975) 972].
- [18] X. Chen, M. -x. Huang, S. Kachru and G. Shiu, JCAP **0701** (2007) 002 [hep-th/0605045].
- [19] F. Arroja, S. Mizuno, K. Koyama and T. Tanaka, Phys. Rev. D **80** (2009) 043527
[arXiv:0905.3641 [hep-th]].
- [20] E. Silverstein and D. Tong, Phys. Rev. D **70** (2004) 103505 [hep-th/0310221].
- [21] M. Alishahiha, E. Silverstein and D. Tong, Phys. Rev. D **70** (2004) 123505
[hep-th/0404084].
- [22] W. Hu, Phys. Rev. D **64** (2001) 083005 [astro-ph/0105117].
- [23] D. M. Regan, E. P. S. Shellard and J. R. Fergusson, Phys. Rev. D **82** (2010) 023520
[arXiv:1004.2915 [astro-ph.CO]].
- [24] S. Mizuno and K. Koyama, JCAP **1010** (2010) 002 [arXiv:1007.1462 [hep-th]].
- [25] K. Izumi, S. Mizuno and K. Koyama, Phys. Rev. D **85** (2012) 023521 [arXiv:1109.3746
[astro-ph.CO]].

- [26] D. M. Regan, arXiv:1112.5899 [astro-ph.CO].
- [27] P. Creminelli, L. Senatore and M. Zaldarriaga, JCAP **0703** (2007) 019 [astro-ph/0606001].